Journal of Power Sources 222 (2013) 161–168

Contents lists available at SciVerse ScienceDirect

Journal of Power Sources

journal homepage: www.elsevier.com/locate/jpowsour

Graphene oxide as auxiliary binder for TiO_2 nanoparticle coating to more effectively fabricate dye-sensitized solar cells

Chin Yong Neo, Jianyong Ouyang*

Department of Material Science and Engineering, National University of Singapore, Singapore 117574, Singapore

HIGHLIGHTS

- Graphene oxide is used as an auxiliary binder in TiO_2 paste.
- Graphene oxide can improve the binding among the TiO_2 nanoparticles.
- Graphene oxide prevents the appearance of crack on TiO_2 films.
- High-quality TiO_2 films can be fabricated from TiO_2–GO pastes via single printing.
- Graphene oxide effectively improve the fabrication of dye-sensitized solar cells.

GRAPHICAL ABSTRACT

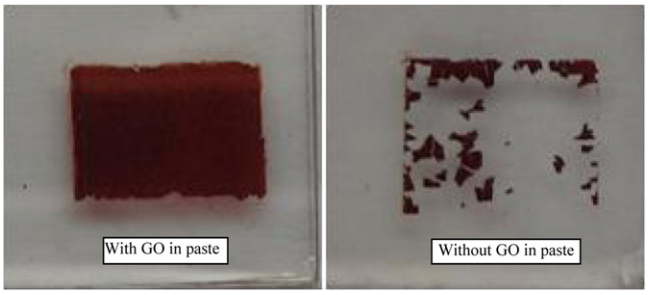

ARTICLE INFO

Article history:
Received 3 July 2012
Received in revised form
22 August 2012
Accepted 24 August 2012
Available online 5 September 2012

Keywords:
Dye-sensitized solar cells
Graphene oxide
Binder
Printing
TiO_2

ABSTRACT

In this paper, we report a novel method to effectively fabricate the mesoporous TiO_2 films of dye-sensitized solar cells (DSCs) by formulating new TiO_2 pastes. Graphene oxide (GO) is added into TiO_2 nanoparticles pastes as an auxiliary binder. Thick mesoporous TiO_2 films free of crack can be prepared by only single printing. TiO_2–GO pastes and films were characterized by dynamic mechanical analysis, X-ray photoelectron spectroscopy (XPS), scanning electron microscopy (SEM), X-ray diffraction (XRD), thermogravimetric analysis (TGA), and FTIR spectroscopy. TiO_2 pastes added with GO exhibit gel behavior. GO helps bind TiO_2 nanoparticles together through the interactions between functional groups on GO and the surface species of TiO_2 nanoparticles. The presence of 0.8 wt.% GO in the TiO_2 paste (GO weight percentage with respect to the weight of TiO_2) is sufficient to fabricate thick and crack-free TiO_2 films via single printing. These mesoporous TiO_2 films fabricated from the TiO_2–GO pastes are investigated as the anode of DSCs. They can give rise to a power conversion efficiency (PCE) of 7.70% for DSCs under AM1.5G illumination, which is almost the same as that of control devices with the TiO_2 mesoporous electrode fabricated from the conventional TiO_2 paste without GO via four-fold printings.

1. Introduction

Dye-sensitized solar cells (DSCs) have attracted considerable attention due to their low fabrication cost and decent power conversion efficiency (PCE) [1–8]. PCE of more than 12% have been reported for DSCs under AM1.5 illumination. They are regarded as the next-generation solar cells. A DSC is a photoelectrochemical device which comprises of a mesoporous TiO_2 photoanode anchored with a monolayer of dye molecules, an electrolyte containing redox species (e.g. I^-/I_3^- redox couple) and a catalytic counter electrode. The working principle of a DSC includes five major steps: (1) photon absorption by the dye molecules and the simultaneous excitation of electrons; (2) electron injection from the excited dye molecules into the TiO_2 photoanode; (3) electron

* Corresponding author. Tel.: +65 6516 1472; fax: +65 6776 3604.
E-mail address: mseoj@nus.edu.sg (J. Ouyang).

0378-7753/$ – see front matter © 2012 Elsevier B.V. All rights reserved.
http://dx.doi.org/10.1016/j.jpowsour.2012.08.075

transport across the mesoporous TiO_2 film to external circuit; (4) dye regeneration by obtaining electrons from the redox species in the electrolyte; and (5) migration of redox species to the counter electrode and the regeneration of the redox species on the catalytic counter electrode. The mesoporous TiO_2 anode plays an important role in the photon-to-electricity conversion. Its quality affects the loading of the dye molecules, the electron injection from the dye molecules to the TiO_2 nanoparticles, and the electron transport across the TiO_2 film to the external circuit [9–12]. A high loading of dye molecules on TiO_2 is needed to harvest more light, which requires a thick mesoporous TiO_2 film. The conventional process to fabricate a mesoporous TiO_2 film is through the wet chemical sol–gel process [13–20]. The final step of the sol–gel process to obtain a mesoporous TiO_2 film involves the sintering at high temperature. At this step, remarkable shrinkage occurs when the gel dries up and the TiO_2 nanoparticles convert to a continuous mesoporous TiO_2 film. The shrinkage causes tensile stress to build up in the TiO_2 film, which can lead to the occurrence of cracks on the TiO_2 layer and de-lamination from the underlying substrate when a thick TiO_2 layer is coated [21–24]. Hence, it is a challenge to fabricate a TiO_2 film thicker than 1 μm via single coating by the sol–gel technique [25,26].

In order to fabricate thick TiO_2 films, organic molecules, such as ethylcellulose [27–29] and ethylene glycol [30–32], are added as binders to formulate the TiO_2 pastes. The chemical structures of ethylcellulose and ethylene glycol are shown in Scheme 1. The weight percentages are usually 50–500 wt.% and 200–450 wt.% with respect to the TiO_2 weight for ethylcellulose and ethylene glycol, respectively. The principle of the binders is related to the interactions between the surface species like –OH groups on the TiO_2 nanoparticles and the hydroxyl groups of the binder molecules. Upon dehydration by heat treatment, the TiO_2 nanoparticles bind together through the formation of Ti–O–R–O–Ti bonds with R as the functional group of the binder. The binder can reduce the tensile stress built up in the TiO_2 films during the sintering and prevent the occurrence of crack and de-lamination, so that thick TiO_2 films can be fabricated [34–36]. Despite the presence of binders in the TiO_2 paste, at least three- or four-fold screen-printings [34] or two-fold doctor blade printings [33] are needed to fabricate crack-free TiO_2 films with a thickness of 10–15 μm that is the optimal thickness for the TiO_2 film of DSCs. Screen printing and doctor blade printing techniques are simple and have advantage of low cost. They are often used for the fabrication of the mesoporous TiO_2 layer of DSCs. If the fabrication of thick TiO_2 films can be achieved via only single printing, the device fabrication will be more effective and labour cost for device fabrication can be reduced.

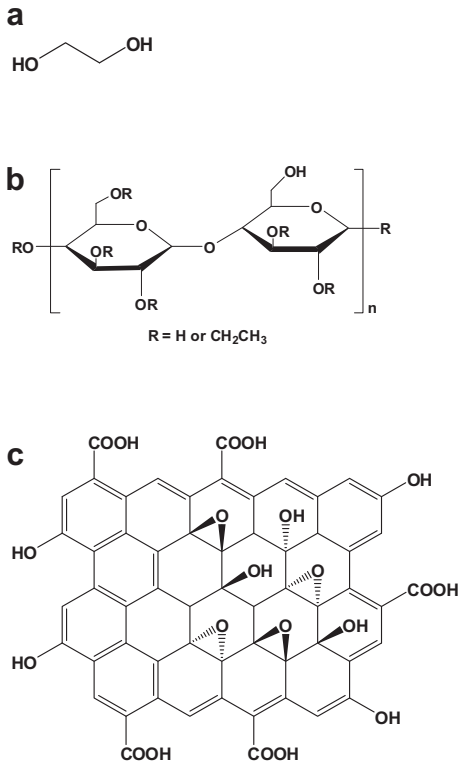

Scheme 1. Structures of (a) ethylene glycol, (b) ethyl cellulose and (c) GO.

In this paper, we report the modification of conventional TiO_2 pastes with the addition of small amount of graphene oxide (GO) as auxiliary binder. This work is different from those reporting the application of graphene in DSCs in literature. Yang et al. [37] blended graphene into the mesoporous TiO_2 layer of DSCs and found that the presence of graphene could improve the PCE of DSCs from 5.01% to 6.97%. Tang et al. [38] also observed that graphene could facilitate the electron transport through the TiO_2 layer of DSCs and it improved the photovoltaic efficiency of DSCs from 0.32% to 1.68%. Ahmad et al. [39] used graphene as an additive in ionic liquid for DSCs and observed that the presence of graphene in ionic liquid electrolyte could improve the PCE of DSCs from 0.16% to 2.10%. Graphene as a carbon nanomaterial can catalyze the regeneration of the redox species in DSCs like carbon nanotubes, carbon fibers and active carbon [2,6,40–44]. It was thus investigated as the counter electrode of DSCs [45–51]. The photovoltaic performance of DSCs with graphene as the counter electrode can be close to that of the control DSCs with Pt as the counter electrode. Different from those works exploiting the conductive and electrocatalytic properties of graphene for DSCs, we use GO as an auxiliary binder to improve the fabrication efficiency of the mesoporous TiO_2 layer, because GO, whose chemical structure is shown in Scheme 1c, has a two-dimensional structure with numerous hydroxyl and carboxylic groups [52–55]. The presence of only 0.8 wt.% GO in TiO_2 paste can give rise to thick and crack-free mesoporous TiO_2 films via single coating. DSCs with mesoporous TiO_2 films fabricated from the TiO_2 pastes added with GO can exhibit a PCE of 7.70%. Hence, this method using GO as auxiliary binder in TiO_2 paste can significantly reduce the fabrication cost of DSCs.

2. Experimental

2.1. Materials

TiO_2 pastes, DSL 18 NR-T (20 nm) and WER2-O (350–450 nm), were purchased from Dyesol. Ruthenium 535-bis TBA (N719) dye and Surlyn (ionomer films of 25 μm thick) were obtained from Solaronix SA. P25 TiO_2 powder (~21 nm particle size, >99.5% trace metals basis), 1-methyl-3-propylimidazolium iodide (PMII) (purity >98%), 4-tert-butylpyridine (TBP) (purity = 99%), tert-butanol anhydrous (purity >99.5%), chloroplatinic acid hexahydrate (H_2PtCl_6), iodine (purity = 99.8%), acetonitrile (purity = 99%), ethyl cellulose (contains 48–49.5% $-OC_2H_5$ groups), α-terpineol (purity >96%), sodium nitrate (purity >99%), potassium permanganate, hydrogen peroxide solution, 98% sulfuric acid and 37% hydrochloric acid were supplied by Sigma Aldrich. Valeronitrile (purity = 99%) and guanidinium thiocynate (purity = 99%), were obtained from Fluka. Natural graphite powder (SP-1 graphite, purity >99.99%) with an average particle size of ~30 μm was purchased from the Bay Carbon Inc. Titanium tetrachloride ($TiCl_4$) was obtained from Merck. All chemicals were used as received.

2.2. Preparation of GO

GO was prepared through a modified Hummer's process [56–60]. In a typical experiment, 1 g graphite powder was mixed with 1 g sodium nitrate in 48 mL 98% sulfuric acid. 6 g potassium permanganate (VII) was gradually added into the mixture under vigorous stirring. This mixture was stirred in an ice bath for 90 min and subsequently in a water bath at 35 °C for 2 h. Then, 40 mL deionized water was dropwise added over 30 min, and the temperature of the mixture rose to 90 °C thereafter. 100 mL deionized water and 10 mL 30% hydrogen peroxide solution were added. GO was collected by centrifugation. It was repeatedly rinsed with 5% HCl solution and successively with deionized water until the solution became neutral. Finally, GO was frozen with liquid nitrogen and freeze-dried with a Labconco Freezone freeze drier for two days.

2.3. Formulation of TiO_2–GO pastes

Two types of TiO_2 pastes were used to formulate the TiO_2–GO pastes. One is the commercial Dyesol DSL 18 NR-T TiO_2 paste. GO was mixed with it by mechanical grinding in an agate mortar for 1 h. These TiO_2–GO pastes are mainly used for the fabrication of mesoporous TiO_2 films for DSCs in this research work.

Home-made TiO_2 pastes were also used to prepare TiO_2–GO pastes. The home-made TiO_2 pastes were prepared according to literature [28,34]. More specifically, the TiO_2–GO pastes were prepared by the following process. At first, 6 g P25 TiO_2 nanoparticles was mixed with 1 mL acetic acid, and the mixture was ground in an agate mortar for 5 min. 5 mL water was slowly added, and the mixture was further ground for 5 min. 30 mL ethanol was subsequently slowly added, and the mixture was ground for 20 min again. Then, the mixture was mixed with 100 mL ethanol and vigorously stirred for 3 min. 20 g α-terpineol was subsequently added into the mixture under vigorous stir. α-terpineol serves as a cosolvent to stabilize the paste. Finally, 3 g ethylcellulose and 30 mL ethanol dispersed with GO were added into the mixture. After the removal of ethanol by the rotary evaporation, the mixture was ground with a three-roller mill. A TiO_2–GO paste was obtained. These TiO_2–GO pastes were mainly used for the characterizations of the pastes and TiO_2 films.

2.4. Fabrication of DSCs

DSCs were fabricated through the conventional process [34]. Fluorine-doped tin oxide (FTO) glass substrates were cleaned successively with detergent, deionized water, acetone and isopropanol. Each cleaning step was carried out in an ultrasonic bath for 15 min. The cleaned FTO glasses were immersed in 40 mM $TiCl_4$ at 70 °C for 30 min and subsequently rinsed with deionized water and ethanol. The TiO_2 working electrode consists of a 13 μm-thick mesoporous TiO_2 film fabricated from the TiO_2–GO pastes formulated by adding GO into the commercial Dyesol DSL 18 NR-T paste and a 2 μm-thick scattering layer of TiO_2 (Dyesol WER2-O) on FTO glass. The mesoporous TiO_2 films were fabricated through the following process. At first, a thick TiO_2 layer was deposited on FTO glass by coating the TiO_2–GO paste via single doctor blade printing. After drying at 125 °C for 6 min, Dyesol WER2-O TiO_2 pastes was coated on the TiO_2 layer via doctor blade. Then, the TiO_2–GO layer together with the Dyesol WER2-O TiO_2 layer were heated in air at 325 °C for 5 min, 375 °C for 5 min, 450 °C for 15 min and 500 °C for 15 min. Finally, they were immersed in 40 mM $TiCl_4$ aqueous solution at 70 °C for 30 min. They were rinsed successively with deionized water and ethanol, and subsequently sintered at 500 °C for 30 min. After cooling down to 80 °C, the TiO_2 work electrodes were immersed into 0.5 mM N719 dye solution in acetonitrile/tert-butanol (volume ratio = 1:1) for 24 h. The dye-impregnated TiO_2 electrode was assembled with a counter electrode, and they were sealed with a Solaronix polymer melt of 25 μm in thickness. The counter electrode was fabricated through the pyrolysis of 0.2 M H_2PtCl_6 in ethanol on FTO glass at 400 °C for 15 min. The cells were filled with an electrolyte comprising 0.6 M PMII, 0.03 M I_2, 0.1 M guanidine thiocynate, and 0.5 M TBP in acetonitrile/valeronitrile (volume ratio = 85:15) cosolvent.

2.5. Characterization of materials and DSCs

Dynamic mechanical analyses were carried out using a Rheometric Scientific Advanced Rheometric Expansion system (ARES) with the dynamic mode. The cone diameter and cone angle were 2.5 cm and 0.04 rad, respectively. The X-ray photoelectron spectra (XPS) were collected with an Axis Ultra DLD X-ray photoelectron spectrometer equipped with an Al Ka X-ray source (1486.6 eV). The resolutions were 1 eV and 0.05 eV for the XPS survey and fine scans, respectively. The CasaXPS version 2.3.14 software was used to subtract the Shirley background, analyze the composition of the materials and deconvolute the XPS peaks. The X-ray diffraction (XRD) patterns were measured with an Advance D8 XRD by Bruker. The FTIR spectra were acquired with a Varian 3100 FTIR spectra. The atomic force microscopic (AFM) and scanning electron microscope (SEM) images were taken using a Veeco Nanoscope IV Multi-Mode AFM with the tapping mode and a Zeiss Supra 40 field emission scanning microscope, respectively. Thermogravimetric analyses (TGA) were performed with a Du Pont 2950 TGA. The samples were heated up to 600 °C at a rate of 10 °C min^{-1} under a constant air flow of 60 cm^3 min^{-1}. The thicknesses of the TiO_2 films were determined using a Tencor P-10 Alpha-Step profiler.

The photovoltaic performances of DSCs were measured with a computer-programmed Keithley 2400 source/meter under a Newport's Oriel class A solar simulator, which simulated the AM1.5G illumination (100 mW cm^{-2}) and was certified to the JIS C 8912 standard. A circular mask with a diameter of 5.2 mm was placed on each DSC during the tests.

3. Results and discussions

3.1. Characterization of TiO_2–GO pastes

Concentrated sulfuric acid and potassium permanganate (VII) are strong oxidants. They can oxidize graphite into graphite oxide. Graphite oxide exfoliates into GO in water. Fig. 1 shows the FTIR spectrum of GO. The FTIR bands at 1733, 1412, 1226 and 1060 cm^{-1} correspond to the vibration modes of C]O, O–H, C–OH and C–O,

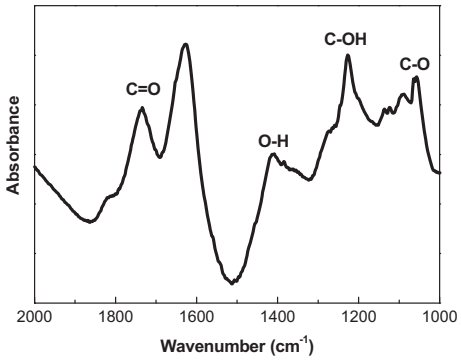

Fig. 1. FTIR spectrum of GO.

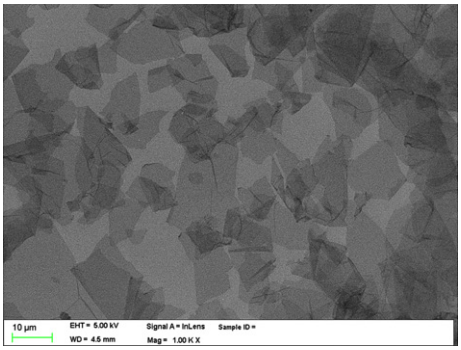

Fig. 2. SEM image of GO sheets.

respectively [61,62]. They confirmed the chemical structure of GO as shown in Scheme 1c.

Fig. 2 shows an SEM image of GO sheets on substrate. It indicates that the GO sheets are generally less than 10 μm. Large GO sheets were investigated by AFM to understand the thickness of an individual GO sheet (Fig. 3). The GO sheet has a thickness of 0.63 nm, which is comparable to that reported in literatures [37,53].

Due to the presence of the functional groups, GO can be dispersed in water and polar organic solvents. It can mix well with TiO_2 pastes. We studied the dynamic mechanical properties of TiO_2 pastes added with GO as the auxiliary binder. Owing to the concern on the possible usage of unknown materials in commercial TiO_2 pastes, we prepared the TiO_2–GO pastes according to literature [28,34]. Fig. 4 illustrate TiO_2 pastes with and without GO. GO turns the color of the TiO_2 paste from white to grey.

Fig. 5 presents the dynamic mechanical analyses of the TiO_2 paste without GO and the TiO_2–0.8 wt.% GO paste. The GO weight percentage is referred to the weight of TiO_2. The storage (G') and loss (G'') moduli are plotted against the angular frequency at two strains of 1% and 10%. G' and G'' are related to the elastic and viscous properties of the materials, respectively [63,64]. For an ideal elastic solid, the applied energy is elastically stored, while the loss modulus is zero. On the other hand, the applied energy is totally lost as heat, whereas the storage modulus is zero for an ideal viscous fluid. The presence of GO significantly affects the dynamical mechanical behavior of the TiO_2 paste. The G' and G'' values of the TiO_2 paste without GO are close in the low frequency regime at both strains, and G'' is greater than G' in the high frequency regime.

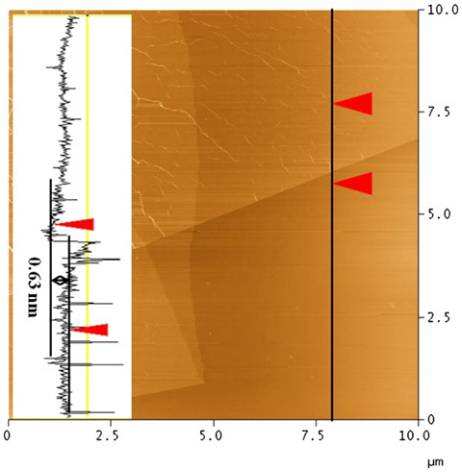

Fig. 3. AFM image of GO sheets.

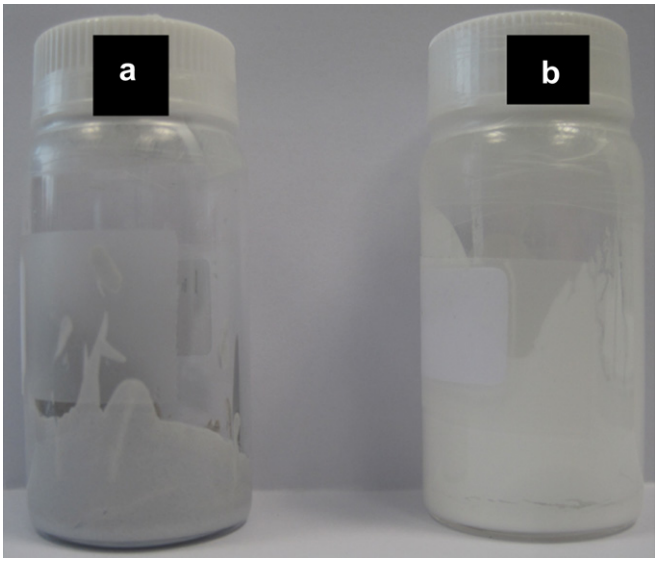

Fig. 4. P25 home-made TiO_2 pastes (a) with and (b) without 0.8 wt.% GO.

These results indicate that the TiO_2 paste without GO behaves as a viscous fluid. In contrast, G' is always greater than G'' in the whole frequency range at both strains for the TiO_2–GO paste. Thus, GO turns the TiO_2 paste into a gel.

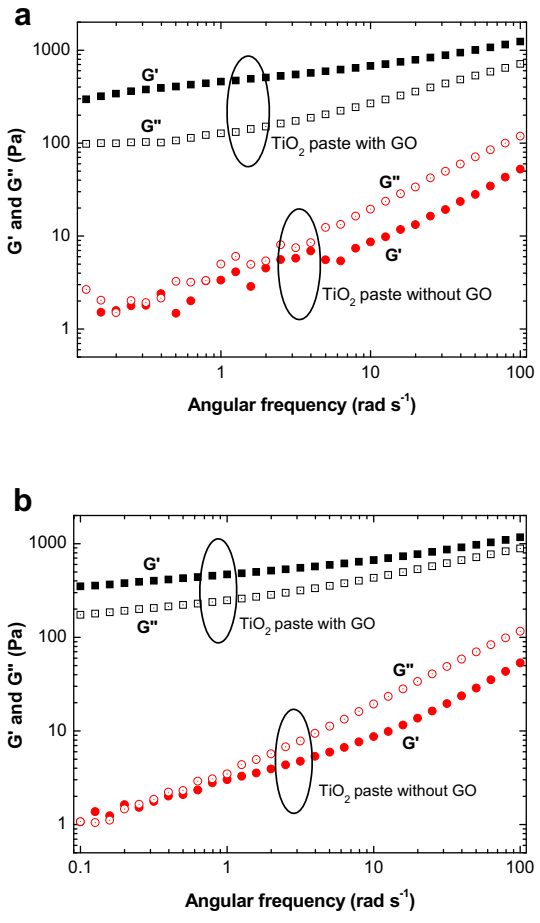

Fig. 5. Dynamic mechanical analyses of P25 home-made TiO_2 pastes with (squares) and without (dots) 0.8 wt.% GO at applied strains of (a) 1% and (b) 10%. G' and G'' are storage and loss moduli, respectively.

The moduli are parameters against the deformation of materials. The increase in G' and G'' of the TiO_2 paste by GO manifests that GO can improve the binding among TiO_2 nanoparticles. Presumably, it is related to the functional groups, including −OH and −COOH, of GO. These groups can form hydrogen bonds with the surface species like −OH of TiO_2 nanoparticles.

3.2. Fabrication of mesoporous TiO_2 films

GO has similar effect on the dynamic mechanical behavior of commercial TiO_2 pastes. The TiO_2 pastes added with different percentages of GO were used for the fabrication of mesoporous TiO_2 films on FTO glass. The TiO_2 films presented in Fig. 6a–d were fabricated via single doctor blade printing and subsequent sintering. The TiO_2 films were impregnated with N719 dye to improve the color contrast of the pictures, as the mesoporous TiO_2 films were semi-transparent. Though each TiO_2 layer prepared by doctor blade is uniform and continuous, the TiO_2 films fabricated from the TiO_2 paste without GO and the TiO_2–0.3 wt.% GO paste are discontinuous, while TiO_2 pastes with 0.8 wt.% and more GO can give rise to crack-free continuous TiO_2 films after the sintering at 500 °C for 45 min. They had a thickness of ~13 μm. The success rate of attaining thick and crack-free TiO_2 films from TiO_2–0.8 wt.% GO paste is 80–90%.

The effect of GO on the quality of the TiO_2 films is remarkable. TiO_2 films fabricated from TiO_2 paste without GO via two- and three-fold doctor blade printings are discontinuous and do not cover the whole area of the substrates (Fig. 6e and f). The thickness of each doctor blade printing via the two- and three-fold printings is approximately 6 μm and 4 μm, respectively, so that the two TiO_2 films have almost the same thickness of 13 μm. The TiO_2 layer was sintered at 125 °C for 6 min after each print. After all the prints, the TiO_2 layer was finally heated in air at 325 °C for 5 min, 375 °C for 5 min, 450 °C for 15 min and 500 °C for 15 min. The cracks are ascribed to the tensile stress in the TiO_2 films during the sintering due to the shrinkage of the films. When the TiO_2 films cannot contain the stress, cracks will occur. This stress increases with the increasing thickness of the films. The TiO_2 films were heated at 125 °C after each print to partially relieve the stress within the TiO_2 films before the next print. We found that a crack-free TiO_2 film of 13 μm thick could be fabricated, only when it was prepared via a four-fold printing. When the TiO_2 films of 13 μm thick are fabricated from TiO_2 paste without GO via one-, two- and three- fold doctor blade printings, the thickness by each print is so large that cracks appear and TiO_2 films do not cover the whole substrate after sintering at 500 °C.

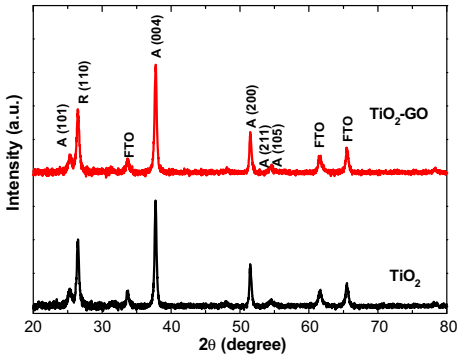

Fig. 7. XRD spectra of mesoporous TiO_2 films fabricated from commercialized DYESOL DSL 18 NR-T TiO_2 pastes with and without 0.8 wt.% GO. A signifies the anatase phase, and R stands for the rutile phase.

The crystallinity of the mesoporous TiO_2 films fabricated from TiO_2 pastes with and without GO was studied by XRD (Fig. 7). The XRD band of anatase (004) is the strongest for both TiO_2 films. There is no appreciable effect of GO on the anatase phase and the crystallinity of the mesoporous TiO_2 films.

The morphology of the TiO_2 films fabricated from TiO_2 pastes with and without 0.8 wt.% GO was studied by SEM. The TiO_2 film fabricated from TiO_2 paste without GO was deposited via a four-fold screen-printings, whereas the TiO_2 film fabricated from TiO_2 paste with 0.8 wt.% GO was deposited by single doctor blade printing. As shown in Fig. 8, both TiO_2 films have almost the same morphology without any appreciable difference.

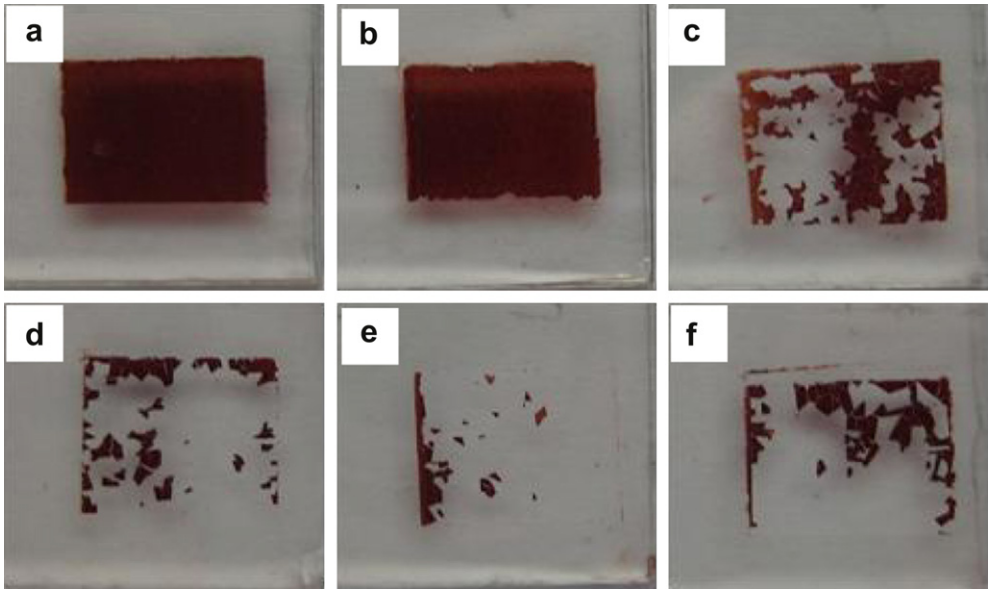

Fig. 6. Dye-impregnated mesoporous TiO_2 films on FTO glass fabricated from commercialized DYESOL DSL 18 NR-T TiO_2 pastes added with (a) 2 wt.%, (b) 0.8 wt.%, (c) 0.3 wt.% and (d) 0 wt.% GO via single doctor blade printing. Dye-impregnated mesoporous TiO_2 films fabricated from the commercialized DYESOL DSL 18 NR-T TiO_2 paste without GO via (e) two- and (f) three-fold doctor blade printings. The TiO_2 films were obtained after coating and subsequently sintering at 500 °C for 30 min. The TiO_2 films were impregnated with N719 dye to improve the color contrast.

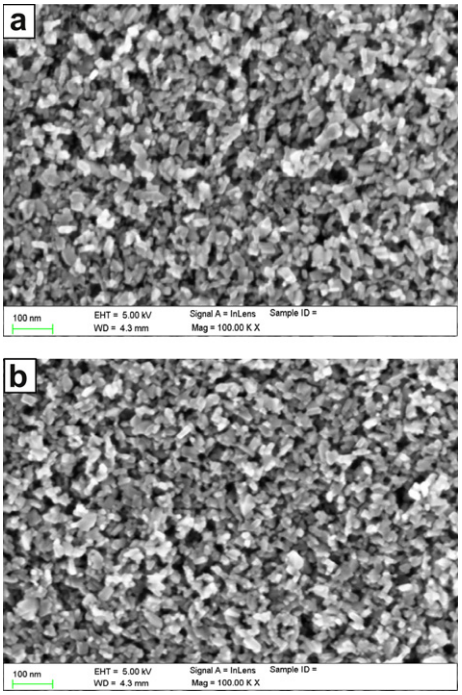

Fig. 8. SEM images of mesoporous TiO_2 films fabricated from commercialized DYESOL DSL 18 NR-T TiO_2 pastes (a) without and (b) with 0.8 wt.% GO.

The compositions of mesoporous TiO_2 films fabricated from TiO_2 pastes with and without 0.8 wt.% GO were analyzed by XPS. As shown in Fig. 9, the addition to GO to the TiO_2 paste has no effect on the Ti 2p XPS bands of the mesoporous TiO_2 film. This implies that there is no chemical reaction between TiO_2 and GO.

Fig. 10 presents the C1s XPS bands of mesoporous TiO_2 films fabricated from the TiO_2 pastes with and without 0.8 wt.% GO. The C1s XPS band for the TiO_2 film fabricated from the TiO_2–0.8 wt.% GO paste is more intense than that from the TiO_2 paste without GO. The difference indicates the remaining of GO decomposition product in the TiO_2 film after the sintering. The XPS spectra suggest that GO decomposition product remaining in the TiO_2 film is approximately 0.1 wt.% (C with respect to TiO_2).

TGA was carried out on GO to understand the decomposition of GO during the sintering. Fig. 11 presents the TGA curve of GO in air from 100 °C to 600 °C at a heating rate of 10 °C min^{-1}. There are two decomposition processes. The one at about 200 °C is due to the pyrolysis of oxygen-containing functional groups [38,45], while the

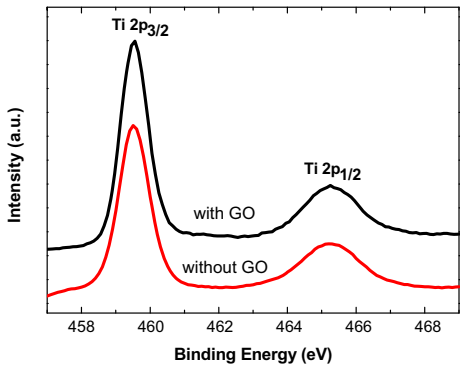

Fig. 9. Ti 2p XPS spectra of mesoporous TiO_2 films fabricated from commercialized DYESOL DSL 18 NR-T TiO_2 pastes with and without 0.8 wt.% GO.

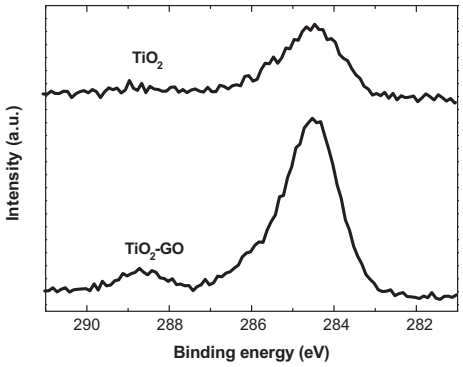

Fig. 10. C 1s XPS spectra of mesoporous TiO_2 films fabricated from commercialized DYESOL DSL 18 NR-T TiO_2 pastes with and without 0.8 wt.% GO.

other one at about 550 °C is the oxidation of sp2 hybridized carbon atoms [37].

The remaining weight is about 50% at 500 °C in terms of the TGA curve as shown in Fig. 11a. But the heating condition for this TGA curve is different from the sintering of TiO_2–GO pastes. GO was also heated from 100 to 500 °C and then held isothermally at 500 °C for 45 min, which were close to the sintering conditions (Fig. 11b). The remnant weighs about 8.5% of the original GO sample. This is consistent with the XPS study on the mesoporous TiO_2 films.

The C1s band of the TiO_2 film fabricated from the TiO_2–0.8 wt.% GO paste is broader than that of the film fabricated from the TiO_2 paste without GO (Fig. 10). It is also remarkably different from that of GO, whereas it is close to that of reduced GO prepared from GO by chemical reduction with Zn (Fig. 12) [39,59]. The XPS spectra indicate that most of the functional groups of GO are removed during the sintering of TiO_2–GO pastes.

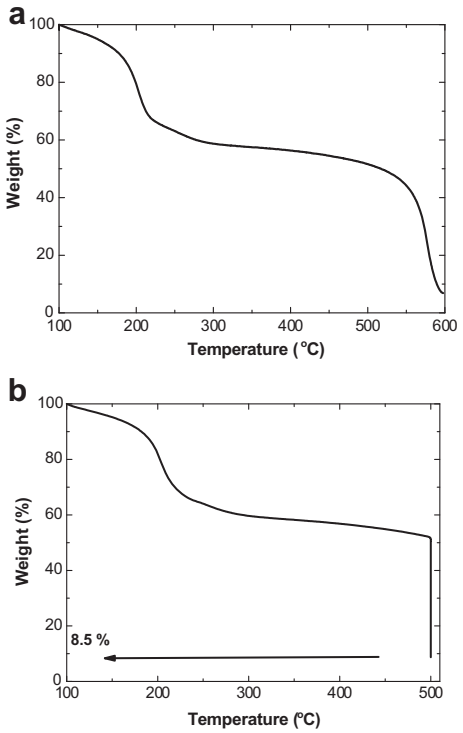

Fig. 11. TGA curves of (a) GO heated from 100 to 600 °C in air and (b) GO heated from 100 to 500 °C in air and then held isothermally at 500 °C for 45 min.

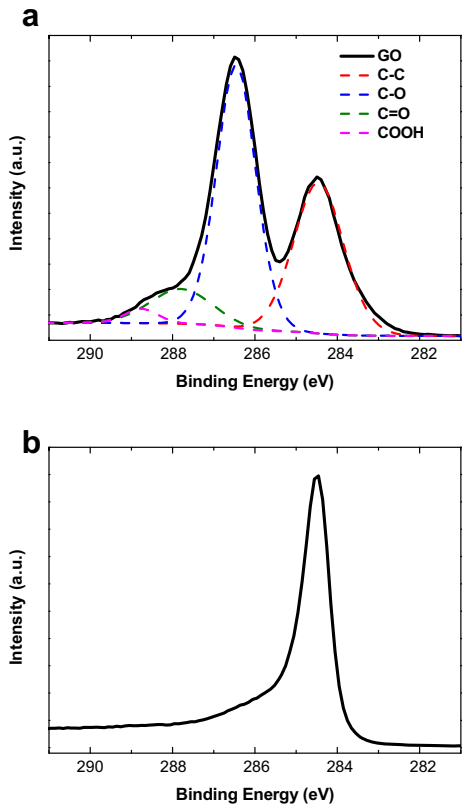

Fig. 12. C 1s XPS spectra of (a) GO and (b) rGO.

3.3. Photovoltaic performance of DSCs

Mesoporous TiO_2 films fabricated from the TiO_2–GO pastes were used as the anode of DSCs. A light scattering TiO_2 layer (WER2-O) was coated on the mesoporous TiO_2 layer by doctor blade to improve the light harvest. The fabrication of the light scattering TiO_2 layer does not introduce any crack to the underlying mesoporous TiO_2 layer. Fig. 13 presents the current density (J)–voltage (V) curve of a DSC with the mesoporous TiO_2 anode fabricated from TiO_2–0.8 wt.% GO paste via single coating. The J–V curve of a control device with the mesoporous TiO_2 anode fabricated from the conventional TiO_2 paste is also presented. The mesoporous TiO_2 anode of the control device was fabricated via four-fold doctor blade printings. The two TiO_2 anodes fabricated from the TiO_2 pastes with and without GO had approximately the same thickness of 13 μm. The photovoltaic performances, including the short circuit current (J_{sc}), open-circuit voltage (V_{oc}), fill factor (FF) and PCE, are summarized in Table 1. The DSC with the TiO_2 fabricated from the TiO_2–GO paste exhibits a PCE of 7.70%, which is the almost same as that of the control DSC. The yield of high-performance DSCs using the TiO_2–GO paste is about 80–90%, almost the same as that using the conventional TiO_2 paste without GO.

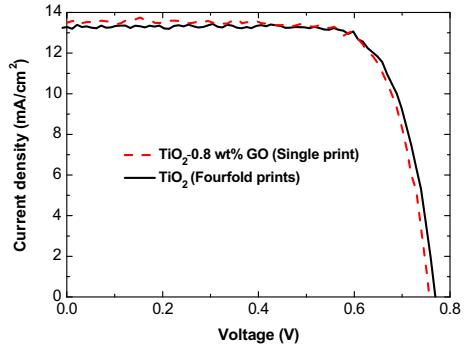

Fig. 13. Current density (J)–Voltage (V) curves of DSCs with the TiO_2 anodes fabricated from TiO_2 and TiO_2–0.8 wt.% GO pastes. The TiO_2 paste used was commercialized DYESOL DSL 18 NR-T TiO2 paste. The mesoporous TiO_2 film from the TiO_2–GO paste was fabricated via single coating, while that from the TiO_2 paste without GO was fabricated via four-fold coatings.

Table 1
Photovoltaic performance of DSCs with the TiO_2 anodes fabricated from TiO_2 and TiO_2–GO pastes. The TiO_2 paste used was commercialized DYESOL DSL 18 NR-T TiO_2 paste. The mesoporous TiO_2 film from the TiO_2–GO paste was fabricated via single doctor blade printing, while that from the TiO_2 paste without GO was fabricated via four-fold doctor blade printings.

Pastes	J_{sc} (mA cm^{-2})	V_{oc} (V)	FF	PCE (%)
TiO_2	13.31	0.77	0.76	7.76
TiO_2–0.8 wt.% GO	13.57	0.76	0.75	7.70

We also investigated DSCs with the mesoporous TiO_2 anode fabricated from the conventional TiO_2 paste via one-, two- or three-fold doctor blade printings for comparison. But these DSCs did not work because the TiO_2 films either were discontinuous or had cracks. The cracks are attributed to the high stress built up within the TiO_2 films as a result of the shrinkage of the films during sintering at 500 °C. Although we mentioned that a thick mesoporous TiO_2 film could be fabricated via two-fold doctor blade printings in the Introduction of this paper, it requires a thin pre-coated TiO_2 layer as a seed layer on FTO glass. No thin TiO_2 seed layer is used for the fabrication of thick mesoporous TiO_2 films from TiO_2–GO pastes in this work. Hence, using small amount of GO as the auxiliary binder in TiO_2 pastes can effectively improve the fabrication of the mesoporous TiO_2 anode whereas it does not affect the photovoltaic efficiency of DSCs.

4. Conclusions

In conclusion, GO can improve the binding among TiO_2 nanoparticles and can serve as an auxiliary binder in TiO_2 pastes. The GO effect is attributed to the interactions between the functional groups of GO and the surface species of TiO_2 nanoparticles. The addition of small amount of GO in TiO_2 pastes enables the fabrication of thick and crack-free TiO_2 films via single print, whereas four-fold printings are needed for TiO_2 pastes without GO. Mesoporous TiO_2 films fabricated from TiO_2–GO pastes are used as the anode of DSCs. The DSCs exhibit similar photovoltaic performance as the control DSCs with mesoporous TiO_2 films fabricated from TiO_2 paste without GO via four-fold printings. The TiO_2–GO paste can effectively improve the efficiency for the device fabrication of DSCs and reduce labour cost.

Acknowledgement

This research work was financially supported by a research grant from the Ministry of Education, Singapore (R-284-000-086-112).

References

[1] M. Gratzel, Acc. Chem. Res. 42 (2009) 1788–1798.
[2] P. Joshi, L. Zhang, Q. Chen, D. Galipeau, H. Fong, Q. Qiao, ACS Appl. Mater. Interf. 2 (2010) 3572–3577.
[3] D. Wu, F. Zhu, J. Li, H. Dong, Q. Li, K. Jiang, D. Xu, J. Mater. Chem. 22 (2012) 11665–11671.
[4] X. Cai, Z. Lv, H. Wu, S. Hou, D. Zou, J. Mater. Chem. 22 (2012) 9639–9644.

[5] E. Dell'Orto, L. Raimondo, A. Sassella, A. Abbotto, J. Mater. Chem. 22 (2012) 11364–11369.
[6] X. Mei, S.J. Cho, J. Ouyang, Nanotechnology 21 (2010) 395202(1)–395202(9).
[7] C.Y. Neo, J. Ouyang, J. Power Sources 196 (2011) 10538–10542.
[8] B. Fan, X. Mei, K. Sun, J. Ouyang, Appl. Phys. Lett. 93 (2008) 143103(1)–143103(3).
[9] M. Gratzel, Inorg. Chem. 44 (2005) 6841–6851.
[10] C.J. Barbe, F. Arendse, P. Comte, M. Jirousek, F. Lenzmann, V. Shklover, M. Grätzel, J. Am. Ceram. Soc. 80 (1997) 3157–3171.
[11] F. Sauvage, D. Fonzo, A. Li Bassi, C.S. Casari, V. Russo, G. Divitini, C. Ducati, C.E. Bottani, P. Comte, M. Grätzel, Nano Lett. 10 (2010) 2567.
[12] A.J. Frank, N. Kopidakis, J. van de Lagemaat, Coor. Chem. Rev. 48 (2004) 1165–1179.
[13] X. Cao, W. Jing, W. Xing, Y. Fan, Y. Kong, J. Dong, Chem. Commun. 47 (2011) 3457–3459.
[14] C. Wang, J.Y. Ying, Chem. Mater. 11 (1999) 3113–3120.
[15] W. Jing, W. Huang, W. Xing, Y. Wang, W. Jin, Y. Fan, Appl. Mater. Inter 1 (2009) 1607–1612.
[16] D. Chen, F. Huang, Y. Cheng, R.A. Caruso, Adv. Mater. 21 (2009) 2206–2210.
[17] J. Yu, X. Zhao, Q. Zhao, Mater. Chem. Phys. 69 (2001) 25–29.
[18] J.T. Park, J.H. Koh, J.A. Seo, J.H. Kim, J. Mater. Chem. 21 (2011) 17872–17880.
[19] D.M. Antonelli, J.Y. Ying, Angew. Chem. Int. Ed. 34 (1995) 2014–2017.
[20] B.B. Lakshmi, P.K. Corhout, C.R. Martin, Chem. Mater. 9 (1997) 857–862.
[21] A. Atkinson, R.M. Guppy, J. Mater. Sci. 26 (1991) 3869–3873.
[22] A.E. Jamting, J.M. Bell, M.V. Swain, L.S. Wielunski, R. Clissold, Thin Solid Films 332 (1998) 189–194.
[23] S. Ito, T. Kitamura, Y. Wada, S. Yanagida, Sol. Energy Mat. Sol. Cells 76 (2003) 3–13.
[24] Y. Zhao, X. Li, Q. Li, C. Deng, J. Mater. Sci. Technol. 27 (2011) 764–768.
[25] B.E. Yoldas, T.W. O'Keefe, Appl. Opt. 18 (1979) 3133–3138.
[26] C.J. Brinker, M.S. Harrington, Sol. Energy Mat. Sol. Cells 5 (1981) 159–172.
[27] J. Nam, E. Lee, W. Jung, Y. Park, B. Sohn, S. Park, J. Kim, J. Bae, Mater. Chem. Phys. 116 (2009) 46–51.
[28] S. Ito, T.N. Murakami, P. Comte, P. Liska, C. Grätzel, M.K. Nazeeruddin, M. Grätzel, Thin Solid Films 516 (2008) 4613–4619.
[29] Z. Wang, H. Kawauchi, T. Kashima, H. Arakawa, Coord. Chem. Rev. 248 (2004) 1381–1389.
[30] W. Wu, G. Zhao, G. Han, B. Song, Mater. Lett. 61 (2007) 1922–1925.
[31] M. Hocevar, U.O. Krasovec, M. Berginc, G. Drazic, N. Hauptman, M. Topic, J. Sol-Gel Sci. Technol. 48 (2008) 156–162.
[32] M. Hocevar, M. Berginc, M. Topic, U.O. Krasovec, J. Sol-Gel Sci. Technol. 53 (2010) 647–654.
[33] S.Y. Huang, G. Schlichtho, A.J. Nozik, M. Grätzel, A.J. Frank, J. Phys. Chem. B 101 (1997) 2576–2582.
[34] S. Ito, M.K. Nazeeruddin, P. Liska, P. Comte, R. Charvet, P. Pechy, M. Jirousek, A. Kay, S.M. Zakeeruddin, M. Grätzel, Prog. Photovolt.: Res. Appl. 14 (2006) 589–601.
[35] N.J. Dahoudi, J. Xi, G. Cao, Electrochim. Acta 59 (2012) 32–38.
[36] Y. Li, W. Lee, D. Lee, K. Kim, N. Park, M.J. Ko, Appl. Phys. Lett. 98 (2011) 103301(1)–103301(3).
[37] N. Yang, J. Zhai, D. Wang, Y. Chen, L. Jiang, ACS Nano 4 (2010) 887–894.
[38] Y.B. Tang, C.S. Lee, J. Xu, Z.T. Liu, Z.H. Chen, Z. He, Y.L. Cao, G. Yuan, H. Song, L. Chen, L. Luo, H.M. Cheng, W.J. Zhang, T. Bello, S.T. Lee, ACS Nano 4 (2012) 3482–3488.
[39] I. Ahmad, U. Khanb, Y.K. Gun'ko, J. Mater. Chem. 21 (2011) 16990–16996.
[40] K.M. Lee, C.W. Hu, H.W. Chen, K.C. Ho, Sol. Energy Mat. Sol. Cells 92 (2008) 1628–1633.
[41] T.N. Murakami, S. ITO, Q. Wang, M.K. Nazeeruddin, T. Bessho, I. Cesar, P. Liska, R. Humphry-Baker, P. Comte, P. Pechy, M. Gratzel, J. Electrochem. Soc. 153 (2006) A2255–A2261.
[42] P. Joshi, Y. Xie, M. Ropp, D. Galipeau, S. Bailey, Q. Qiao, Energy Environ. Sci. 2 (2009) 426–429.
[43] Z. Huang, X. Liu, K. Li, D. Li, Y. Luo, H. Li, W. Song, L. Chen, Q. Meng, Electrochem. Commun. 9 (2007) 596–598.
[44] Y. Luo, D. Li, Q. Meng, Adv. Mater. 21 (2009) 4647–4651.
[45] G. Zhu, L. Pan, T. Lu, T. Xu, Z. Sun, J. Mater. Chem. 21 (2011) 14869–14875.
[46] H. Choi, H. Kim, S. Hwang, Y. Han, M. Jeon, J. Mater. Chem. 21 (2011) 7548–7551.
[47] D.W. Zhang, X.D. Li, H.B. Li, S. Chen, Z. Sun, X.J. Yin, S.M. Huang, Carbon 49 (2011) 5382–5388.
[48] L. Kavan, J.H. Yum, M. Gratzel, ACS Nano 5 (2011) 165–172.
[49] J.D. Roy-Mayhew, D.J. Bozym, C. Punckt, I.A. Aksay, ACS Nano 4 (2010) 6203–6211.
[50] M.Y. Yen, C.C. Teng, M.C. Hsiao, P.I. Liu, W.P. Chuang, C.C.M. Ma, C.K. Hsieh, M.C. Tsai, C.H. Tsai, J. Mater. Chem. 21 (2011) 12880–12888.
[51] H. Zheng, C.Y. Neo, X. Mei, J. Qiu, J. Ouyang, J. Mater. Chem. 22 (2012) 14465–14474.
[52] C. Virojanadara, M. Syväjarvi, R. Yakimova, L.I. Johansson, Phys. Rev. B 78 (2008) 245403(1)–245403(6).
[53] S. Stankovich, D.A. Dikin, G.H.B. Dommett, K.M. Kohlhaas, E.J. Zimney, E.A. Stach, R.D. Piner, S.T. Nguyen, R.S. Ruoff, Nature 442 (2006) 282–286.
[54] V.C. Tung, J.H. Huang, J. Kim, A.J. Smith, C.W. Chu, J. Huang, Energy Environ. Sci. 5 (2012) 7810.
[55] D. Krishnan, F. Kim, J. Luo, R. Cruz-Silva, L.J. Cote, H.D. Jang, J. Huang, Nano Today 7 (2012) 137–152.
[56] X. Mei, J. Ouyang, Carbon 49 (2011) 5389–5397.
[57] H. Cao, B. Li, J. Zhang, F. Lian, X. Kong, M. Qu, J. Mater. Chem. 22 (2012) 9759–9766.
[58] V.H. Pham, H.D. Pham, T.T. Dang, S.H. Hur, E.J. Kim, B.S. Kong, S. Kim, J.S. Chung, J. Mater. Chem. 22 (2012) 10530–10536.
[59] X. Sun, J. He, J. Tang, T. Wang, Y. Guo, G. Li, H. Xue, Y. Hu, Y. Ma, J. Mater. Chem. 22 (2012) 10900–10910.
[60] X. Mei, H. Zheng, J. Ouyang, J. Mater. Chem. 22 (2012) 9109–9116.
[61] Y. Si, E.T. Samulski, Nano Lett. 8 (2008) 1679–1682.
[62] S. Stankovich, R.D. Piner, S.T. Hguyen, R.S. Ruoff, Carbon 44 (2006) 3342–3347.
[63] X. Mei, J. Ouyang, Langmuir 27 (2011) 10953–10961.
[64] X. Mei, J. Ouyang, Carbon 48 (2010) 293–297.